
VICCA: VISUAL INTERPRETATION AND COMPREHENSION OF CHEST X-RAY ANOMALIES IN GENERATED REPORT WITHOUT HUMAN FEEDBACK

Sayeh GHOLIPOUR PICHA

Univ. Grenoble Alpes,
CNRS, Grenoble INP, GIPSA-lab,
38000 Grenoble, France

sayeh.gholipour-picha@grenoble-inp.fr

Dawood AL CHANTI

Univ. Grenoble Alpes,
CNRS, Grenoble INP, GIPSA-lab,
38000 Grenoble, France

dawood.al-chanti@grenoble-inp.fr

Alice CAPLIER

Univ. Grenoble Alpes,
CNRS, Grenoble INP, GIPSA-lab,
38000 Grenoble, France

alice.caplier@grenoble-inp.fr

January 30, 2025

ABSTRACT

As artificial intelligence (AI) becomes increasingly central to healthcare, the demand for explainable and trustworthy models is paramount. Current report generation systems for chest X-rays (CXR) often lack mechanisms for validating outputs without expert oversight, raising concerns about reliability and interpretability. To address these challenges, we propose a novel multimodal framework designed to enhance the semantic alignment and localization accuracy of AI-generated medical reports. Our framework integrates two key modules: a Phrase Grounding Model, which identifies and localizes pathologies in CXR images based on textual prompts, and a Text-to-Image Diffusion Module, which generates synthetic CXR images from prompts while preserving anatomical fidelity. By comparing features between the original and generated images, we introduce a dual-scoring system: one score quantifies localization accuracy, while the other evaluates semantic consistency. This approach significantly outperforms existing methods, achieving state-of-the-art results in pathology localization and text-to-image alignment. The integration of phrase grounding with diffusion models, coupled with the dual-scoring evaluation system, provides a robust mechanism for validating report quality, paving the way for more trustworthy and transparent AI in medical imaging.

Keywords Chest X-ray Localization · Chest X-ray Image Generation · Chest X-ray Interpretability

1 Introduction

Recent advancements in using multimodal data by integrating textual data with images in the medical domain have revolutionized diagnostic workflows in AI-driven healthcare Yildirim et al. [2024], Chen et al. [2024], mirroring trends in natural image analysis. Among these advancements, large language models (LLMs) and Visual Language Models (VLMs) have shown considerable growth in processing and generating text from text and image, excelling in applications such as conversational AI and image captioning. Despite the popularity of LLMs and VLMs in natural image processing, their application in medical imaging remains in its early stages, with only a handful of studies exploring this synergy in the medical field Müller et al. [2024], Bannur et al. [2024]. For instance, using VLMs in medical image captioning

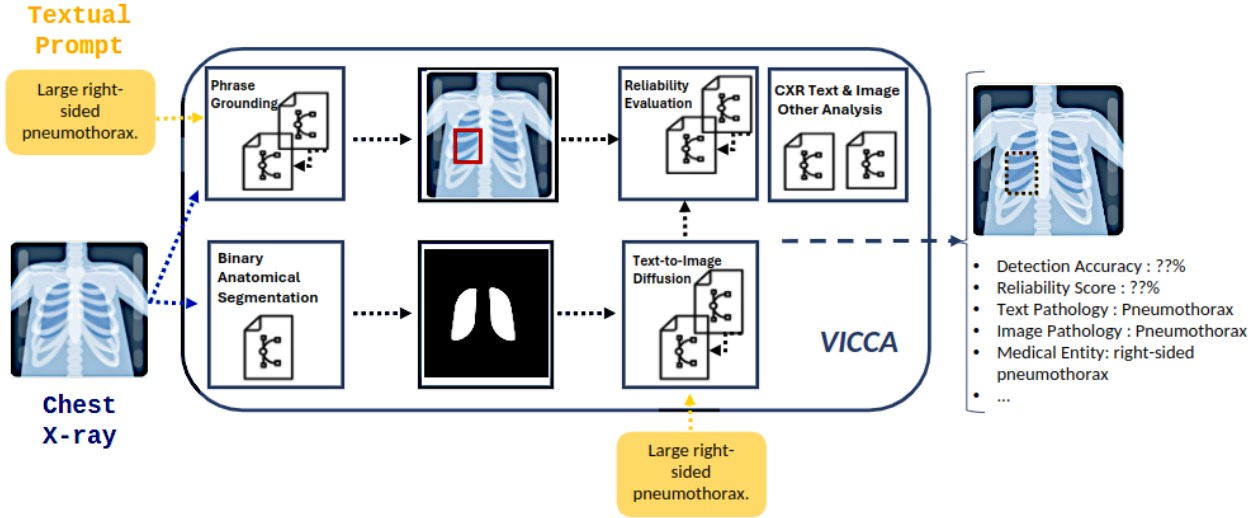


Figure 1: Overview of VICCA. Given a chest X-ray image and a text query, the model performs visual localization of the text input and generates a comprehensive set of information. This includes the localization accuracy, the alignment accuracy between the visual output and the text query, the presence of the specified pathology in both the text query and the chest X-ray image, the identification of the main entity within the text prompt, and a summarization of the text input into its key medical entities.

using text and image data has shown great potential for enhancing diagnostic accuracy Bannur et al. [2024], enabling richer contextual understanding Müller et al. [2024], and supporting more precise decision-making. These models offer the potential to generate detailed and contextually relevant medical reports from images. However, unlike image captioning in natural data, medical reports require an in-depth understanding of domain-specific terminology, the ability to interpret subtle pathological features, and an alignment with structured medical reporting standards Romaissa et al. [2022], Selivanov et al. [2023], Boecking et al. [2022], Huang et al. [2021] to ensure the generated information is clinically relevant and contextually accurate. Nonetheless, using textual information alongside medical images introduces additional complexity, potentially increasing the challenges of interpretability and trust in automated systems as errors or ambiguities in generated reports could lead to misdiagnosis or mistrust among practitioners Yildirim et al. [2024]. This complexity underscores the need for innovative frameworks to ensure reliability and facilitate validation.

Addressing the lack of quantifiable validation metrics in AI-generated medical reports, including quantifiable metrics that ensure alignment and consistency between textual and visual data, provides a more robust foundation for clinicians to evaluate and rely on these outputs. Even though integrating multimodal data introduces additional complexity, it also enables the development of a double-mapping approach—linking information across modalities—that facilitates a deeper understanding of the relationship between image features and corresponding textual descriptions.

While our work focuses on chest X-rays (CXR) due to the availability of datasets and the critical need for advancements in radiology, LLMs and VLMs have also been applied in other medical domains, such as MRI for brain tumor analysis and ultrasound for fetal health assessment. These applications highlight the growing importance of multimodal AI in healthcare, showing its potential to integrate various data sources for improved diagnostic insights. The framework we propose offers a generalizable solution that could be extended to other modalities, further advancing AI’s role in healthcare.

In the context of Chest X-ray (CXR) analysis, few studies Müller et al. [2024], Tanida et al. [2023], Bannur et al. [2024] have focused on improving automated report generation by detecting abnormalities in CXR images and producing structured, clinically relevant reports based on identified regions of interest (ROI). However, these AI-generated reports often are not self-explanatory and do not include standardized metrics to evaluate their trustworthiness. Consequently, expert validation remains imperative, and the trustworthiness of these reports continues to be a significant concern. This issue is further complicated by the variability in current methods for CXR report generation, particularly in how differently they contextualize and structure content to address clinical terms. To address these limitations in AI-generated medical reports, our research introduces a novel and comprehensive multimodal framework that enhances the visual interpretability, reliability, and consistency of generated reports. Unlike previous approaches, this framework not only integrates multimodal data but also introduces a unique evaluation metric designed to quantify the trustworthiness and reliability of these reports. Our approach leverages report content to localize pathologies within imaging data and

validates these localizations through a complementary AI module, which generates synthetic images from text data. By comparing the consistency of ROIs from the localization across modalities, the framework produces quantitative confidence scores, reinforcing the reliability of the outputs.

Our multi-modalities model operates as follows: The phrase grounding model processes a CXR image along with a corresponding text prompt describing the pathologies. It outputs bounding boxes that localize the identified pathologies within the image. Subsequently, a stable diffusion model takes the same text prompt and a binary anatomical mask derived from the original CXR image as input to generate a new synthetic CXR image. This generated image retains the original anatomical structure while incorporating the pathology described in the prompt.

To evaluate the consistency and accuracy of the generated outputs, we register the previously detected bounding boxes onto the synthetic image and assess the ROIs compatibility using feature-based similarity metrics. This process results in two distinct scores:

1. **Detection Accuracy:** Quantifies the probability of the alignment between the localized regions and the report content, ensuring accurate text-to-image correspondence, and providing a measure of the visualization validity for text-to-image localization.
2. **Reliability Score:** A novel interpretability score that verifies whether the localized features align with the semantic meaning of the report. This is achieved through text-to-image generation techniques that produce new CXR images while preserving anatomical structure. Assessing the feature consistency of the ROIs between generated and original images which contains the most important information regarding the anomaly/pathology.

The rationale behind this approach lies in detecting potential errors in the generated reports. If the report inaccurately describes features not present in the original CXR image, these discrepancies will manifest in the synthetic image generated from the report’s content. Consequently, the compatibility between the original and synthetic images in their respective ROIs will be low, signaling potential inaccuracies in the report’s generated features. This dual-scoring mechanism ensures a robust evaluation of both localization precision and semantic alignment, enhancing the trustworthiness of AI-generated reports.

In our approach, we designed a novel validation system for our pipeline that does not rely on expert feedback, addressing challenges such as limited accessibility, high costs, and the occasional subjectivity of expert opinions. Instead, we leveraged annotated datasets and established evaluation metrics to ensure an objective and reproducible validation process. This system is adaptable across diverse databases, enhancing the generalizability and robustness of our model evaluation. Furthermore, our framework validates each model in the pipeline individually, focusing on their medical understanding, covering both anatomy and pathology and their overall performance.

The output of our pipeline also includes additional spatial information about the image pathology, derived from the TorchXRyVision model Cohen et al. [2022]. Furthermore, it extracts text pathology and medical entities from the input text using our previous model Picha et al. [2024], comparing the interpretability of both the visual and textual data.

Our primary contribution is the introduction of a novel cross-validating multimodal pipeline that can be broken down into the following points:

1. **Primary Model:** We fine-tuned and modified a phrase grounding model originally trained on natural image datasets to adapt its architecture for medical chest X-ray (CXR) applications. To enhance its performance, we integrated a BERT-like encoder Devlin et al. [2019], Boecking et al. [2022], pre-trained on CXR report texts, and further optimized it to complement the architecture effectively.
2. **Image Generation:** A stable diffusion model is developed for text-to-image generation Dhariwal and Nichol [2021], Zhang et al. [2023]. This model generates CXRs from input text reports while preserving the anatomical structure of the original image. To ensure anatomical integrity, a binary mask segmented from the lung regions of the original CXR guides the generation process, maintaining alignment with the underlying medical context.
3. **Medical Validation:** A validation method has been developed to assess the anatomical and pathological accuracy of the generated CXRs. This is achieved either by leveraging existing well-known models or by training specialized AI models with high accuracy customized to the task. The approach ensures that the generated images are both realistic and clinically relevant.
4. **Feature Similarity Validation:** To assess the similarity of regional bounding boxes between the original and generated images, we introduce a false report with no resemblance to the original report in thoracic disease and use it to generate CXR images. The goal is to observe whether the distribution of the feature changes as a result.

By making these contributions, we have advanced the integration of multimodal models in medical imaging, thereby enhancing both the generation and interpretability of medical reports and images.

2 Related Work

This project introduces a novel pipeline for interpretability in chest X-ray report generation, for better comparison we break down the pipeline into key components—Medical Phrase Grounding and Chest X-ray Text-to-Image Diffusion—corresponding to methods used in related studies. We will next discuss each module and its limitations within the medical context then compare our results with these individual components and validate the pipeline’s final output accordingly.

2.1 Medical Phrase Grounding

Phrase grounding models focus on locating specific findings or phrases described in text within medical images. Works such as Boecking et al. [2022], Chen et al. [2023], Vilouras et al. [2024] demonstrate the utility of these approaches for identifying anomalies. For instance, Boecking et al. [2022] propose a zero-shot method that maps textual findings to ROIs in CXRs. Similarly, Chen et al. [2023] highlight challenges in locating small or overlapping findings, particularly where visual and textual cues may conflict. Despite their progress, these models primarily serve as localization tools and often lack mechanisms to validate their outputs without expert feedback. This limits their reliability in practical clinical settings. Additionally, their generalizability is constrained due to limited medical training data compared to natural image datasets.

Alternatively, Grounded reporting methods Ichinose et al. [2023], Tanida et al. [2023], Müller et al. [2024], Zou et al. [2024] extend phrase grounding by combining localization with automated report generation. These methods aim to improve the accuracy and clinical relevance of generated reports by first detecting regions of interest and then generating textual descriptions. For example, Tanida et al. [2023] demonstrate that grounded approaches outperform direct image-to-text generation in identifying multiple anomalies. While grounded reporting improves report precision, the generated reports still face challenges in terms of interpretability and validation. Moreover, these methods primarily focus on generating new reports rather than enhancing existing ones.

In contrast to previous approaches, our work leverages medical phrase grounding to localize findings described in a given CXR report, focusing on enhancing the interpretability and trustworthiness of existing AI-generated reports rather than creating new ones. By accurately mapping textual findings to their corresponding ROIs in the image, this method facilitates visual validation and bridges the gap between textual and visual modalities. Furthermore, the introduction of a dual scoring system quantifies interpretability, transforming trust from a binary agree/disagree metric into a measurable level of performance, thereby enabling greater confidence in the AI’s outputs.

Unlike models trained predominantly on natural image datasets Liu et al. [2023], our architecture is fine-tuned using medical data, ensuring it is specifically adapted to the unique complexities of CXR images, such as subtle anatomical structures and overlapping pathologies. To address the challenges posed by the limited availability and subjectivity of expert feedback, we incorporate a validation pipeline that utilizes annotated datasets and standardized metrics. This provides a robust and objective evaluation framework, ensuring both reliability and clinical relevance in the assessment process.

2.2 Chest X-ray text to image Diffusion

Text-to-image diffusion models represent a novel approach in medical imaging by generating synthetic CXR images from textual reports. These models operate by mapping text descriptions to visual features, effectively synthesizing images that align with the described pathologies and anatomical context. This process can enhance medical image analysis by addressing issues such as data scarcity, enabling augmentation, and supporting research validation. Despite their promise, current methods face challenges in maintaining anatomical consistency—a critical requirement for clinical applicability.

Pioneering works like RoentGen Chambon et al. [2022a] and Cheff Weber et al. [2023] have demonstrated the potential of generating CXRs directly from free-form text reports. While these methods can produce plausible images, they often lack control over critical spatial features, resulting in inconsistencies in the anatomical structure. For example, a generated image describing “left lung consolidation” might misplace the pathology or alter unrelated anatomical regions, thereby reducing clinical reliability Chambon et al. [2022b], Rombach et al. [2021].

Class-conditional X-ray generation approaches, such as Packhäuser et al. [2022], address privacy concerns with advanced sampling strategies but primarily focus on dataset augmentation rather than preserving anatomical detail. While useful for specific tasks, such methods do not fully meet the needs of structured, pathology-guided image generation, particularly when spatial accuracy is critical. In our earlier work Gholipour Picha. et al. [2023], we highlighted the importance of using synthetic data to balance datasets effectively, underscoring that, for our research,

preserving anatomical structure in chest X-rays is essential, particularly when incorporating spatial information like pathology.

A more recent study, XReal Hashmi et al. [2024], takes a significant step forward by employing anatomy and pathology masks to guide X-ray generation. This ensures the precise placement of pathologies while maintaining organ-level accuracy. However, the reliance on detailed pathology masks introduces a dependency on expert input, which may limit scalability when using only textual CXR reports.

Our guided image generation employs binary lung segmentation masks and medical text prompts to validate the contextual fidelity of prompts by ensuring anatomical accuracy and consistent localization of pathologies. The generated images aim to validate the output of earlier modules in our pipeline, specifically the phrase grounding model, by quantifying the consistency between the original image and its synthesized counterpart in the region of interest.

By integrating these components, the interconnected pipeline ensures mutual validation across modules, enhancing trustworthiness in the AI pipeline and addressing the limitations that exist in these modules.

3 Methods

In this research, we designed a multimodal pipeline consisting of two key modules, as shown in Figure 2. Our primary method involves localizing the input text prompt within CXR images using medical phrase grounding techniques. This step identifies regions of interest (ROIs) corresponding to the described pathologies, forming the foundation for assessing the alignment between textual and visual data. Subsequently, the remaining components focus on validating the semantic content and reliability of the prompt by indirectly assessing features within the generated image. We designed an auxiliary module—a diffusion model—capable of generating synthetic CXR images based on the input text prompt. This model ensures fidelity to the anatomical structure of the original CXR image while accurately reflecting the prompt’s content into visual features. These features are used to support and validate the semantic meaning of the prompt. By generating images with pathologies similar to those described in the text, this approach facilitates a detailed comparison between the original and synthetic CXRs, allowing for a robust evaluation of the consistency between text and image pathologies.

Ultimately, this pipeline produces a comprehensive set of outputs, both visual and textual, accompanied by dual scores, one assessing visual accuracy and the other evaluating semantic alignment. These scores provide critical insights into the reliability of the report aiding specialists in their decision-making process.

3.1 Chest X-ray Phrase Grounding

Our goal in using a phrase grounding model specialized for chest X-ray data is to localize pathology features described in the input text report to their corresponding regions on the image, providing a visual representation as the first step in the interpretability process. We employ Grounding Dino Liu et al. [2023], a state-of-the-art model designed for phrase grounding in natural images. This model excels in associating textual descriptions with specific regions of interest, leveraging its advanced architecture for precise localization.

3.1.1 Grounding Dino for Natural Images

The Grounding DINO architecture is designed for grounded object detection, integrating visual and textual understanding. It begins with a backbone, such as a ResNet or Swin Transformer, which extracts multi-scale features from the input image. These features are then processed by a transformer encoder, employing multi-head self-attention to capture global contextual relationships across the image.

A transformer decoder takes the encoded features and object queries, which are learnable embeddings, to decode information for predicting object regions and their alignment with textual descriptions. A separate text encoder, often derived from a pretrained language model like BERT Devlin et al. [2019], processes the input text query, embedding it into a feature space aligned with the visual representations.

The model employs multimodal alignment to ensure that the embeddings of corresponding text and image elements share a unified feature space, typically using a contrastive learning approach. Predictions are made through specialized heads: one for bounding box localization and another for scoring the alignment between textual queries and detected objects. The training process uses a Hungarian matching loss for object-query assignments, a box regression loss for refining bounding boxes, and a grounding loss to enforce accurate text-object associations. This architecture enables robust performance in tasks requiring simultaneous visual and textual reasoning.

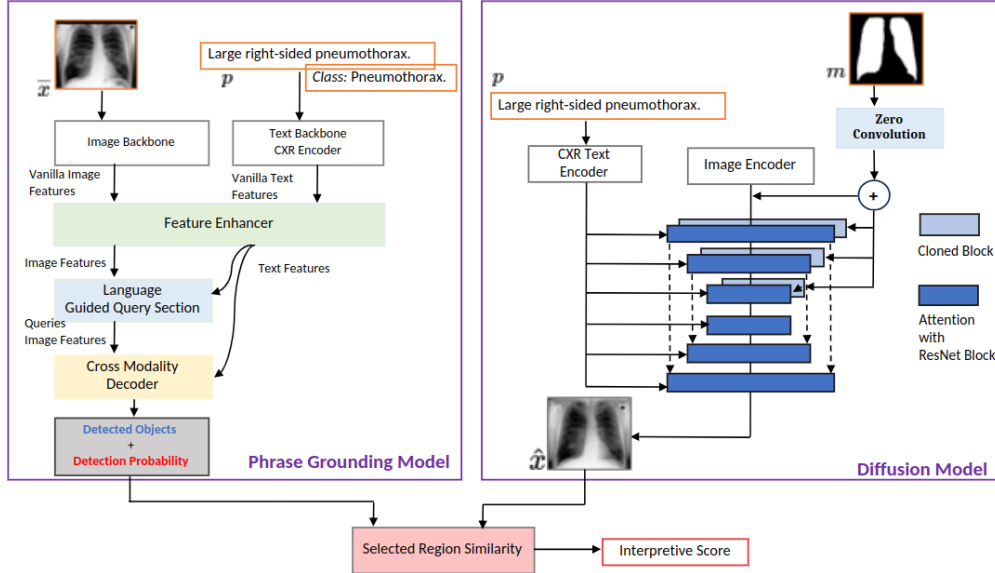


Figure 2: Overview of the model pipeline: It comprises one primary model (phrase grounding) and two auxiliary models (Stable Diffusion Model and Regional Text Generation). The pipeline takes three inputs: the image (\bar{x}), pathology text (p), and a binary mask (m). The output includes a localization or box loss and a contrastive loss for the pathology text. The output of the Stable Diffusion Model is represented as \hat{x} , which should closely approximate the original input image ($\bar{x} \approx \hat{x}$). The “zero convolution” is 1×1 convolution with both weight and bias initialized to zeros. It serves as a way to integrate the encoded text with the encoded guided binary mask, ensuring the output maintains anatomical structural fidelity.

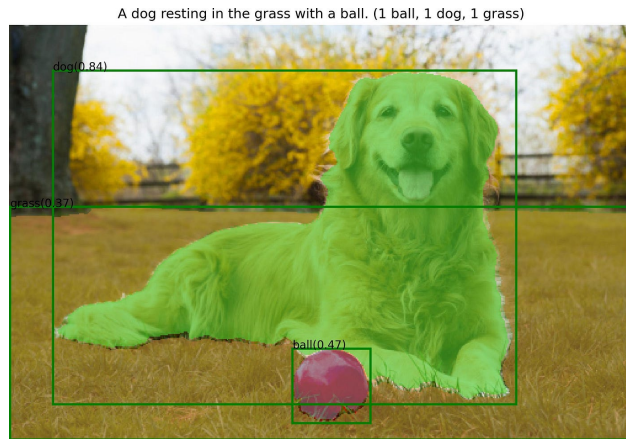


Figure 3: An example of phrase grounding using the Grounding Dino model Liu et al. [2023] on a natural image. The output includes localization bounding boxes for all objects mentioned in the text that are present in the image, along with their associated detection probabilities.

Figure 3 demonstrates an example of using the Grounding Dino model for the phrase grounding task. The model processes a natural language prompt (“A dog resting in the grass with a ball”) and localizes the described objects—one dog, one patch of grass, and one ball—within the associated image, generating corresponding bounding boxes for each identified region.

3.1.2 Adapting Grounding Dino to Medical Contexts

While Grounding Dino is highly effective for natural images, its direct application to medical imaging is challenging due to the unique demands of the domain. Medical phrase grounding requires precise spatial alignment and the ability to interpret subtle pathological features, which are often absent in natural datasets. Furthermore, adapting such



Figure 4: An example of phrase grounding using the Grounding Dino model trained exclusively on natural data with the phrase “Cardiomegaly with mild pulmonary vascular congestion”. The model inaccurately localizes the entire image as the detected object.

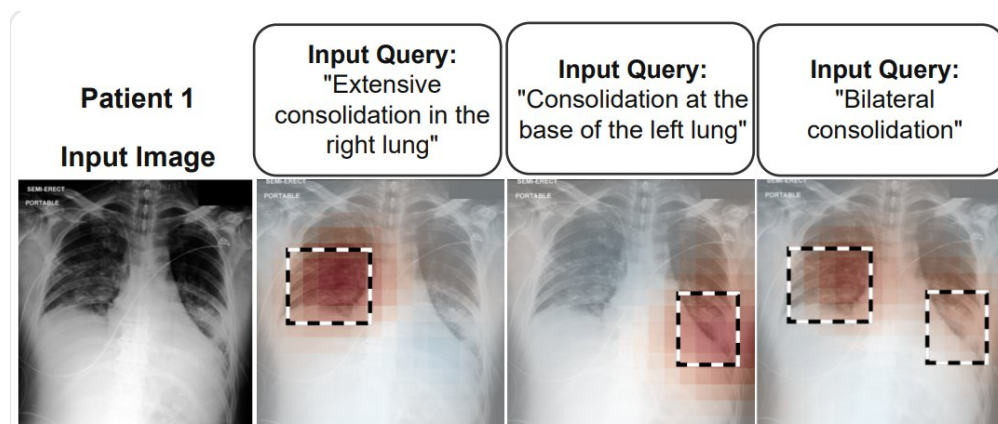


Figure 5: A well-annotated dataset for phrase grounding, featuring bounding box locations, associated text queries, and corresponding pathology descriptions Boecking et al. [2022].

models necessitates fine-tuning with annotated medical data, including bounding boxes for pathologies and detailed text descriptions. Figure 4 present a chest X-ray image grounded to the phrase “Cardiomegaly with mild pulmonary vascular congestion” using the Grounding Dino model trained on natural data. Despite the simplicity of the medical prompt and the accessibility of the text features for even non-experts, the model incorrectly identifies the entire image as the object. This highlights the challenge of capturing subtle pathological features in medical imaging, underscoring the need for domain-specific adaptations.

We fine-tuned Grounding Dino on CXR datasets to overcome these challenges, customizing it for medical applications. For this process, we used two key datasets:

1. MS-CXR Dataset Boecking et al. [2022] A specialized dataset designed for phrase grounding tasks, as illustrated in Figure 5. It contains 1,162 annotated CXR images, each paired with detailed bounding box annotations and corresponding pathology descriptions, making it a valuable resource for developing and evaluating phrase grounding models. However, the dataset’s limited size poses a challenge, as it is insufficient for training a conventional object detection model. This necessitates strategies such as few-shot learning or the incorporation of additional datasets to ensure robust model performance.

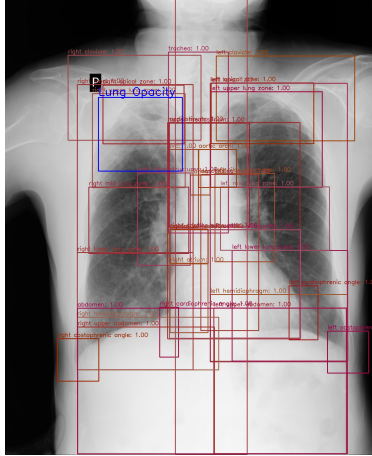


Figure 6: An example CXR image from the VinDr-CXR dataset. The blue bounding box represents the dataset-provided annotation for the pathology present in the image. The red bounding boxes indicate the anatomical regions automatically detected by our trained model.

2. VinDr-CXR Dataset Nguyen et al. [2022] A larger dataset with over 18,000 subjects’ annotated images, providing bounding box locations for 17 common thoracic diseases. However, VinDR-CXR lacks detailed written reports associated with each subject, which is critical for our phrase grounding purposes.

One potential solution to this issue is the use of automated report generation models to create descriptive reports. However, as our goal is to enhance the interpretability of such models, we opted not to include them during training to avoid introducing potential biases. Instead, we enhanced the dataset by associating pathologies with their anatomical regions to enrich the spatial information.

To enrich the VinDr-CXR dataset for phrase grounding tasks, we developed a method to associate pathologies with precise anatomical regions. This was achieved using the DETR (DEtection TRansformer) model Carion et al. [2020], a state-of-the-art object detection framework, and the chest ImaGenome dataset Wu et al. [2021], which defines 36 anatomical regions in chest X-rays (CXR).

DETR combines a convolutional neural network backbone with a transformer architecture, offering several advantages, such as its ability to generate unique predictions without relying on traditional post-processing steps like non-maximum suppression. These unique predictions make DETR particularly suited for detecting overlapping and closely spaced regions, which are common in medical imaging tasks.

The model was originally pretrained on natural images. However, its transformer-based architecture and end-to-end training pipeline make it adaptable to complex medical datasets. For our study, we retrained DETR on the chest ImaGenome dataset, which provides high-quality bounding box annotations for anatomical regions. This adaptation leverages DETR’s global attention mechanism, enabling precise identification of anatomical structures, even when these regions are subtle or overlap significantly. Figure 6 shows an example output, where bounding boxes in red represent automatically detected anatomical regions.

Since the VinDr-CXR dataset provides pathology labels and their corresponding bounding boxes but lacks anatomical descriptors, we enriched the dataset by associating each pathology label with the closest anatomical region. This was achieved using empirical distance and intersection over union (IoU) metrics. For instance in the case of Figure 6, A bounding box labeled “Lung Opacity” that overlaps most with the “right upper lung zone” was annotated as “Lung Opacity in right upper lung zone”. This refinement significantly improves the granularity and spatial context of the dataset, making it more suitable for tasks requiring precise alignment between text and image features. Moreover, this approach can be considered a frugal model, leveraging existing datasets and computational resources efficiently while minimizing dependency on extensive new data annotations. Such a framework can enhance a wide range of medical imaging tasks, including detection, segmentation, and classification.

Given that this research does not involve direct radiologist feedback, we manually verified 200 samples by referencing existing radiology descriptors¹ to ensure the accurate association of pathologies with anatomical regions. Based on this validation, we recalibrate the automated augmentation process for the remaining dataset, ensuring consistency and

¹www.radiologymasterclass.co.uk

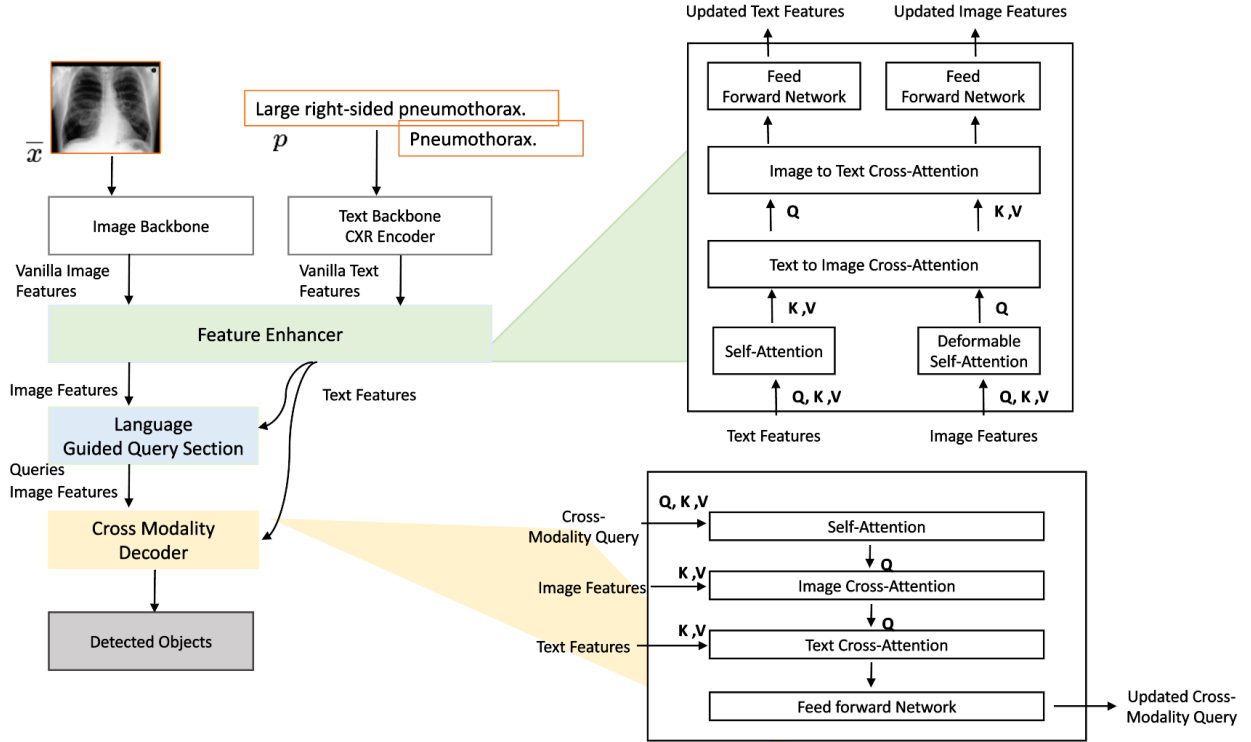


Figure 7: The architecture of the Grounding DINO model integrates the BiomedVLP-CXR-BERT as the text encoder for medical text attention. This model grounds the provided text input onto the image using cross-attention maps between the image and text.

reliability across all annotations. For instance, our initial approach primarily assigned each pathology to the closest and most overlapped anatomical region. However, in cases of bilateral pathologies, this method could result in one side being excluded. To address this, we refined the model to account for bilateral occurrences by considering both left and right regions when they overlap with the pathology’s bounding box.

The fine-tuning process involved few-shot training, using a subset of annotated images to adapt the model’s weights to the medical domain while preserving its pretrained capabilities for natural data. This step is critical to balance generalization and domain-specific accuracy.

3.1.3 Model Architecture and Fine-Tuning

As shown in Figure 7, we fine-tuned Grounding Dino’s architecture in the following components:

- Language Encoder tokenizes and embeds textual prompts for semantic representation. Grounding Dino’s use BERT encoder Devlin et al. [2019], a text encoder pretrained on English language using a masked language modeling (MLM) objective, empirically proven powerful for natural language tasks, equipped with a large token vocabulary. However, numerous tokens in this vocabulary are not relevant to the medical domain. Despite efforts to integrate models such as ClinicalBERT Huang et al. [2019], specifically trained for medical applications, into Grounding DINO’s training process, this did not result in notable enhancements in feature extraction. To overcome these limitations, we integrated BiomedVLP-CXR-BERT Boecking et al. [2022], a text encoder specifically trained on chest X-ray reports. By leveraging BiomedVLP-CXR-BERT in the fine-tuning process, we aligned the text encoder’s outputs more closely with the medical context, significantly enhancing localization outcomes.

By integrating the BiomedVLP-CXR-BERT encoder into the Grounding DINO model, we effectively transformed the previously natural language outputs into medically contextualized ones. This adjustment resulted in a substantial performance enhancement. Specifically, the general DETR-like loss during training decreased from 35.85 when using the BERT encoder to 8.79 when using the BiomedVLP-CXR-BERT encoder. Figure 8 shows the training loss progression for both encoders. Using the specialized BiomedVLP-CXR-BERT encoder not only resulted in a significant loss reduction but also achieved faster convergence during training.

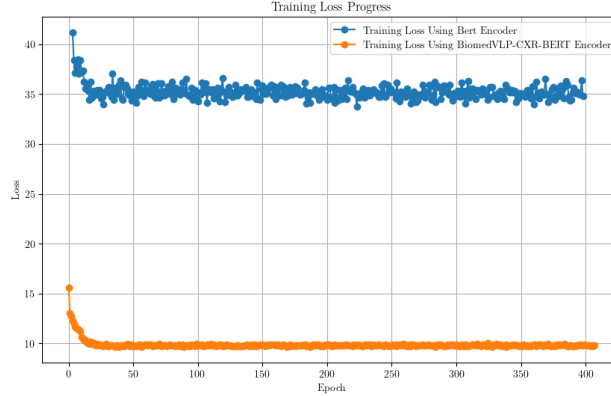


Figure 8: Training loss progression for the phrase grounding model using two text encoders (BERT and BiomedVLP-CXR-BERT). The specialized BiomedVLP-CXR-BERT encoder, designed for CXR text, significantly reduces the loss and achieves faster convergence compared to using the BERT encoder.

- Image encoder processes input images to extract relevant visual features. Grounding Dino supports both ResNet He et al. [2016] and Swin Transformer Liu et al. [2021] architectures as backbones. For our fine-tuning, we employed only the Swin Transformer due to its superior performance on high-resolution images and its patch-merging strategy, which effectively aligns text and image features both globally and locally. This choice proved particularly advantageous for the intricate spatial details required in chest X-ray analysis.
- Loss Function: We adopted the original loss configuration of Grounding Dino, which includes L1 loss and Generalized Intersection over Union (GIoU) for bounding box regression Zhang et al. [2022]. The model also employs a contrastive loss to associate predicted objects with their corresponding classifications. This process involves computing the dot product between each query and text feature, generating logits for each text token, and applying focal loss Lin et al. [2017] to these logits. For fine-tuning, a multi-task loss function combining localization loss (L1 and GIoU) and classification loss (focal loss) was utilized. Training was conducted over 400 epochs, with hyperparameters such as learning rate and batch size optimized via grid search. The final model exhibited a stable loss convergence with the loss stabilizing around 8.7, ensuring both precise localization and robust classification capabilities.

Success in the phrase grounding task provides the first score in our dual-scoring mechanism, offering a detection accuracy metric for each bounding box. Table 1 presents a case study using the optimized Grounding DINO model with two different textual inputs. The CXR image was annotated with the accurate diagnosis of “Cardiomegaly with mild pulmonary vascular congestion,” achieving a bounding box detection accuracy of 76%. Conversely when exposed to an unrelated prompt, “Left-sided Pulmonary Edema,” the accuracy dropped significantly to 20%, localizing an anomaly in the left lung but failing to identify edema. This result highlights the model’s capability to differentiate and accurately localize the correct pathology when provided with a relevant text prompt while demonstrating a reduced performance for unrelated or incorrect prompts.

While our enhancements improve the visual interpretability of the text report, the model’s outputs still require radiologist validation to ensure reliability and comprehensive accuracy. To address this limitation and achieve independence from expert feedback in this research, we introduce an auxiliary model specifically designed to evaluate the reliability and accuracy of the bounding box localizations.

To ensure proper alignment between the text prompt and the image content—where the text accurately describes the image and the image features validate the prompt’s meaning, we introduce a reliability score. This score quantifies the alignment, providing an objective measure to assess the trustworthiness of the model’s outputs.

3.2 Auxiliary Model: Stable Diffusion for CXR Generation with Anatomy Preservation

We introduce an auxiliary model to enhance the reliability of the visual interpretation of the text report. Specifically, we utilize a CXR generation model to produce an alternative CXR image that is anatomically similar to the original but guided by the input text report. This approach provides an additional set of CXR images that can be compared to the localized regions in the original image. The comparison allows us to evaluate the report’s accuracy and its alignment with the image by determining whether the report provides sufficient spatial detail—such as pathology and anatomical

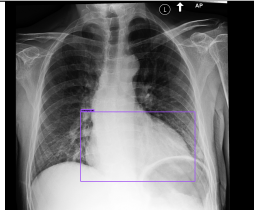
Input	Cardiomegaly with mild pulmonary vascular congestion.	Left-sided Pulmonary Edema.
Output		

Table 1: The results of the phrase grounding model using two different text prompts. The ground truth report, “Cardiomegaly with mild pulmonary vascular congestion,” got the bounding box detection with 76% accuracy. The last column shows the results with a random prompt, “Left-sided Pulmonary Edema,” which achieved a bounding box accuracy of 20%.

regions. If accurate, the localized regions in the original CXR image should closely align with the corresponding areas in the generated images.

Given that most thoracic diseases occur within or near the lung region as visible on chest X-rays, and to ensure the preservation of anatomical structures similar to the original image, we extracted the lung segmentation from the original image. This was achieved using an existing model ².

Using the binary lung segmentation image and the input text report, we generated a chest X-ray image through a stable diffusion model originally designed for text-to-image synthesis. By incorporating inpainting techniques, we integrated the binary image into the training process to suit our specific purpose. For this task, we built upon the stable diffusion model (SD1.5), leveraging its pretrained weights to retain its understanding of general tokens. We then adopted the ControlNet model architecture Zhang et al. [2023] as the backbone and integrated a BiomedVLP-CXR-BERT encoder for tokenizing chest X-ray entities.

The final architecture of the model is illustrated in Figure 2 diffusion model. Similar to the stable diffusion model, ControlNet uses an autoencoder architecture for text-to-image generation. However, in ControlNet, additional cloned encoder blocks are introduced to process the binary image, providing control over the inpainting process. While the original encoder blocks learn, the cloned blocks are frozen, and vice versa. A zero-convolution layer is then used to link the cloned blocks with the locked model, enabling smooth integration and enhanced control.

The model was fine-tuned to adapt to CXR data effectively. The training was implemented over 25 epochs, achieving a training loss of 0.078 and a validation loss of 0.125, indicating a stable convergence.

Table 2 presents four samples generated using our method. In the third row, the generated images are shown, which result from feeding the binary lung masks and their paired text reports (from the MIMIC-CXR dataset) into the model. The final row illustrates generated images created using the same binary masks but paired with random, unrelated reports. One challenge observed in these generations is the presence of artifacts around the periphery of the images. While these artifacts are random and irrelevant to the study’s focus, they do not affect our main objective, as we concentrate on the lung regions and their associated pathologies. The trained model demonstrates strong capabilities in preserving anatomical structures. For example, in the fourth sample, the right lung in the original image is completely opaque. However, when paired with a random report that does not describe this opacity, the model still synthesizes it accurately, highlighting its robustness in anatomical reconstruction.

For a clearer demonstration of the model’s performance with varying reports, Table 3 presents an additional example. The middle column displays an image generated using the ground truth report, while the last column shows an image generated using a random, unrelated report. Images generated with the ground truth report closely resemble the original input image, while those generated with incorrect pathology descriptions do not. Notably, when provided with a random report mentioning “cardiomegaly,” the model expanded the heart region in the generated image, reflecting its ability to interpret and map text input to corresponding anatomical features effectively.

²<https://github.com/IlliaOvcharenko/lung-segmentation.git>

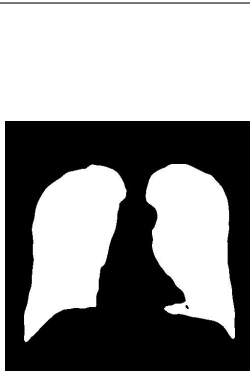
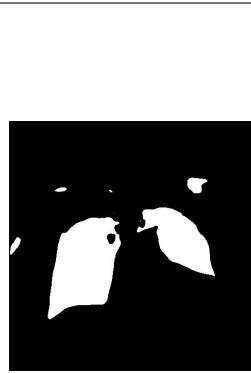
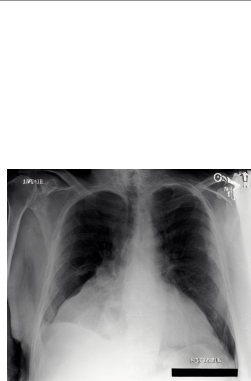
Original Image				
Binary Image Lung Segmentation				
Generated with the Original Report	 Similarity with the GT: 88.6%	 Similarity with the GT: 85.3%	 Similarity with the GT: 78.6%	 Similarity with the GT: 81.9%
Generated with A False Report	 Similarity with the GT: 84.2%	 Similarity with the GT: 79.6%	 Similarity with the GT: 72.7%	 Similarity with the GT: 67.3%

Table 2: The results of the CXR generative model using two different text prompts. The ground truth report is in the middle column and a random CXR report is in the last column. Feature similarity is used to calculate the generation's similarity with the Ground Truth (GT) image.

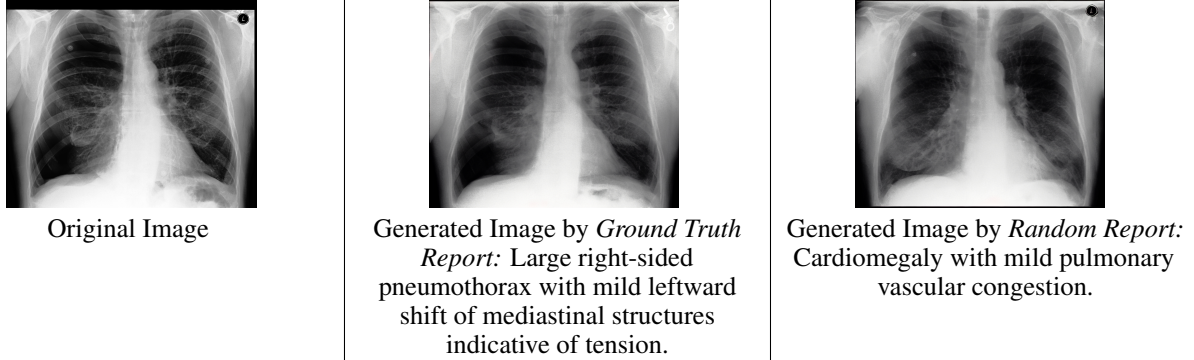


Table 3: The results of the CXR generative model using two different text prompts. The ground truth report is in the middle column and a random CXR report is in the last column.

Phrase Grounding Model			
Dataset	Train	Validation	Test
MS-CXR Boecking et al. [2022]	817	169	176
VinDr-CXR Nguyen et al. [2022]	34367	3000	2697
Stable Diffusion			
MIMIC-CXR Johnson et al. [2019a]	207827	2991	2189
Automatic Lung Segmentation			
Chest ImaGenome Wu et al. [2021]	166521	23593	47393

Table 4: Dataset distribution used for training and validation across the models, including the number of images and associated annotations.

Accurately generating features from text enables a robust comparison of feature-level similarity within regions of interest, facilitating the evaluation of the reliability score and validating the alignment between the report and the image.

4 Training Protocols and Datasets

Each model was trained independently using different datasets. Table 4 summarizes the distribution of training and validation datasets for each model, detailing the number of images and their associated annotations. Across all models, only chest X-ray images in the Posterior-Anterior (PA) or Anterior-Posterior (AP) views were included, while those in the lateral view were excluded. Additionally, images labeled as “No Finding” in the VinDr-CXR dataset were excluded from the training process.

In the case of the MIMIC-CXR dataset, which contains approximately 53,000 images labeled as “No Finding”, we excluded 20,000 of these images. This adjustment was made to balance the dataset more effectively with other pathology labels, ensuring equal representation during training.

5 Result and Validation

To effectively evaluate the entire pipeline, it is crucial to first assess each component individually. While achieving state-of-the-art performance would be ideal, our primary focus is on achieving results that are reasonably close to existing benchmarks. This is because each model’s contribution we made is essential for the overall evaluation and functionality of the complete pipeline.

5.1 Chest X-ray Phrase Grounding

The standard approach for evaluating a phrase grounding model involves mean Average Precision (mAP) for token understanding and mean Intersection over Union (mIoU) for object detection. To this end, we evaluated the model

VinDr-CXR		
Model	mAP \uparrow	mIoU \uparrow
ChEX Müller et al. [2024]	14.12 \pm 0.95	-
BioVIL Boecking et al. [2022]	2.82 \pm 0.25	-
VICCA (Ours)	34.36 \pm 1.79	38.32 \pm 2.7
MS-CXR		
ChEX Müller et al. [2024]	44.47 \pm 2.21	47.52 \pm 1.45
TransVG Deng et al. [2021]	44.05 \pm 2.63	53.51 \pm 1.53
BioVIL Boecking et al. [2022]	18.62 \pm 1.37	28.57 \pm 1.31
VICCA (Ours)	41.67 \pm 0.69	55.27 \pm 2.36

Table 5: Phrase Grounding model performance against VinDR-CXR and MS-CXR datasets.

Model	MS-SSIM \uparrow	Dice \uparrow	FID \downarrow
Cheff Weber et al. [2023]	0.415	0.5	24.64
RoentGen Chambon et al. [2022a]	0.386	0.631	82.14
XReal Hashmi et al. [2024]	0.701	0.838	55.12
VICCA (Ours)	0.71	0.841	35.76

Table 6: The comparison of FID scores among three models. Our results indicate that our model achieved the second-best score.

using the test sets of two datasets, with detailed information provided in Table 4. For the VinDr-CXR dataset, captions were generated based on the pathology and the closest associated anatomical region. The mAP is calculated using the probability scores for each detection, and the results are summarized in Table 5.

The results for the VinDr-CXR dataset, presented in Table 5, reflect the performance of benchmark models on the object detection task. Since our method of generating captions based on anatomical regions and pathologies is a novel contribution, direct comparisons with other models for the phrase grounding task were not possible. Nevertheless, our approach outperformed the benchmark models on the test set for object detection in this dataset.

For the MS-CXR dataset, the results pertain to the phrase grounding task. Our model achieved comparable performance to the benchmarks in terms of mAP and surpassed them in mIoU. These findings highlight the effectiveness of our model for CXR phrase grounding tasks, demonstrating its capability to localize and interpret pathologies with high precision.

5.2 Stable Diffusion for CXR Generation

To evaluate the generative model, we compared its performance against benchmark models using three metrics: Multi-Scale Structural Similarity Index (MS-SSIM), Dice score, and Fréchet Inception Distance (FID). These metrics collectively assess the quality and anatomical fidelity of the generated images.

For the evaluation, we generated 10 samples for the 2,065 reports in the test set, resulting in a total of 20,650 generated images. The results, presented in Table 6, show that our model achieved the second-best FID score while outperforming all benchmarks in MS-SSIM and Dice. These outcomes demonstrate the superior quality of our model’s generated images, particularly in preserving anatomical structures.

The results highlight the effectiveness of our inpainting technique during training, demonstrating that a model originally trained on natural images can be successfully adapted for CXR images by utilizing binary lung segmentation to maintain anatomical consistency and a specialized text encoder for medical contexts. In comparison, the Cheff model with the best FID score, generates images solely based on text input, and lacks this anatomical precision. Furthermore, our model surpassed the performance of the XReal model, which also focuses on preserving anatomical accuracy, further validating our approach.

While the quantitative metrics used are valuable for validating the generative model’s performance, the sensitivity of the medical domain necessitates a deeper focus on medical validation. Since this study does not involve collaboration with radiologists or expert feedback, ensuring the model’s medical reliability becomes paramount.

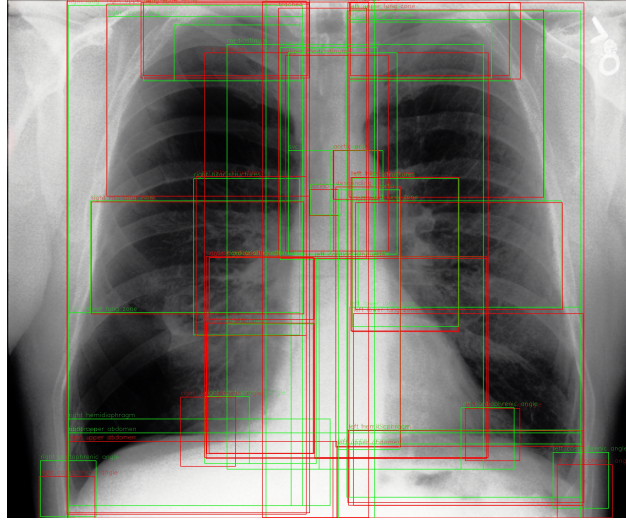


Figure 9: Ground truth anatomical regions in green and automatic detection of the anatomical regions on generated CXR in red. The mIoU of the bounding boxes is 76%.

Before evaluating the entire pipeline, it is crucial to validate the generative model specifically through medical criteria, as it serves as a reference for assessing localization accuracy. To ensure the robustness of the generated outputs, we developed a novel system designed to evaluate the anatomical and pathological aspects of the model. This additional validation ensures that the generated images align with the medical standards required for accurate interpretation and assessment.

5.3 Validation Process

The validation process for the generative model in this research is inspired by the way experts acquire knowledge. It centers on evaluating the fundamental aspects of anatomical regions and correlating the anomalous parts of the image with the corresponding pathology. Consequently, our first step is to establish a method for validating the anatomical structures of the generated images. This ensures that the generated outputs maintain consistency with real CXR anatomical accuracy.

5.3.1 Anatomical Validation

A typical chest X-ray (CXR) image consists of approximately 36 distinct anatomical regions, such as the "right upper lung zone," "right mid lung zone," "right atrium," "descending aorta," "carina," "left upper abdomen," and others. Identifying these anatomical regions is a straightforward task, thanks to the availability of the Chest ImaGenome dataset Goldberger et al. [2000], Wu et al. [2021], which provides radiologist-annotated bounding boxes for these 36 regions within the MIMIC-CXR dataset. Leveraging this dataset, we successfully trained a robust region detector using the DETR model Carion et al. [2020]. A notable advantage of the DETR model is its capacity to detect all class objects simultaneously, which is particularly useful given the close proximity of anatomical features in CXR images. The model demonstrated rapid convergence, achieving a DETR-like loss of 3.5030 and a generalized **IoU loss** of 0.29 after just 14 epochs. On the test set, the IoU accuracy reached an impressive 76%.

Subsequently, we applied the trained DETR model to the generated CXRs to obtain bounding boxes and evaluated their IoU against the ground truth. The IoU score for the generated CXR set was 68%, validating the generative model's effectiveness in preserving anatomical structures. Figure 9 demonstrates the performance of the trained DETR model on a generated CXR image. The red bounding boxes represent the automatically detected anatomical regions, while the green bounding boxes depict the ground truth annotations from the Chest ImaGenome dataset. Since generated images often contain slight spatial shifts compared to ground truth images, we addressed this by aligning the bounding boxes based on the superior vena cava (SVC) region, which is typically central in CXR images. By detecting the positional shift of the SVC in both images, we adjusted the bounding boxes accordingly. The mean Intersection over Union (mIoU) score between the detected and ground truth bounding boxes is 76.2%, indicating a high degree of overlap and alignment for the majority of anatomical regions.

5.3.2 Pathological Validation

To validate the pathological accuracy of the generated CXR images, we utilized the TorchXrayVision library for pathology classification Cohen et al. [2022]. While various datasets provide annotations for 14 to 15 thoracic diseases, many existing classification models are either outdated or limited to a subset of these classes. TorchXrayVision overcomes these limitations by leveraging multiple datasets for comprehensive pathology classification. Using this library, we classified the pathologies in the generated CXRs and compared the detected pathologies’ accuracy with those in the original images. The generative model achieved an average classification accuracy of 88.53% on the generated test set.

These results highlight our generative model’s capability to produce CXR images that accurately reflect pathological features while maintaining anatomical fidelity.

5.4 Pipeline Result

Figure 10 presents an example result from our pipeline. Alongside the two scoring metrics—detection accuracy and reliability score—the pipeline also provides additional spatial information regarding the pathology extracted from the input text using our previous model Picha et al. [2024], which identifies relevant medical entities as well. The image pathology is classified using the TorchXRyVision model Cohen et al. [2022], which categorizes CXR images into 14 pathology classes. Since both the original image and the prompt are derived from the MIMIC-CXR dataset, we also include CheXpert pathology annotations Irvin et al. [2019] from the official dataset for comparison.

5.5 Pipeline Evaluation

With the generative model validated and the phrase grounding model demonstrating good precision based on quantitative results, we can now address the primary goal of this research, providing a reliability score for the automatically localized regions.

To achieve this, we translate the bounding boxes from the phrase grounding model onto the generated images, ensuring the exact same regions are evaluated. An encoder trained specifically on chest X-ray images was then used to extract features from these bounding box regions. To evaluate the similarity between the original and generated regions, we use a twofold approach. First, we analyzed the pixel-level features by calculating the Multi-Scale Structural Similarity (MS-SSIM). Then, using an image encoder trained specifically on CXR images to extract high-level features and computed the χ^2 value as a quantitative measure of correspondence.

Since no direct reference exists for this evaluation, we designed a two-step methodology to interpret both the MS-SSIM and χ^2 metrics effectively:

1. Using the Original Report:

- Bounding boxes were detected based on the original report, and both MS-SSIM and χ^2 values were calculated by comparing the corresponding regions in the original and generated images.
- A χ^2 value closer to zero indicates high feature similarity, while an MS-SSIM value closer to one signifies a strong structural resemblance between the regions.

2. Using a Random Report:

- The process was repeated using a random report unrelated to the original image.
- The expectation was that the MS-SSIM values would be significantly lower, and the χ^2 values significantly higher, confirming reduced similarity between the localized and generated regions when the report did not correspond to the actual content.

Figure 11 illustrates the results of this comparison based on the average MS-SSIM and the χ^2 values.

For MS-SSIM, the similarity scores based on the Real Report (RR) indicate a narrower range, with outliers remaining close to the margins, indicating a consistent and high degree of similarity. In contrast, the scores based on the False Report (FR) show a wider distribution, with a noticeably lower average similarity, reflecting the reduced alignment between the generated and original images in this scenario. The higher similarity scores observed can be attributed to the method used for selecting random reports, which was based on pathology annotations from the MIMIC-CXR dataset. Random reports were considered acceptable if they lacked any explicit similarity to the original reports. However, in certain cases, overlapping visual traits between pathologies—for instance, “lung opacity” and “nodule”—led to unintentional correlations. These shared visual characteristics in the selected random reports contributed to the detection of higher similarity scores.

Original Prompt

Enlarged cardiac silhouette is accompanied by pulmonary vascular congestion and diffuse interstitial edema.

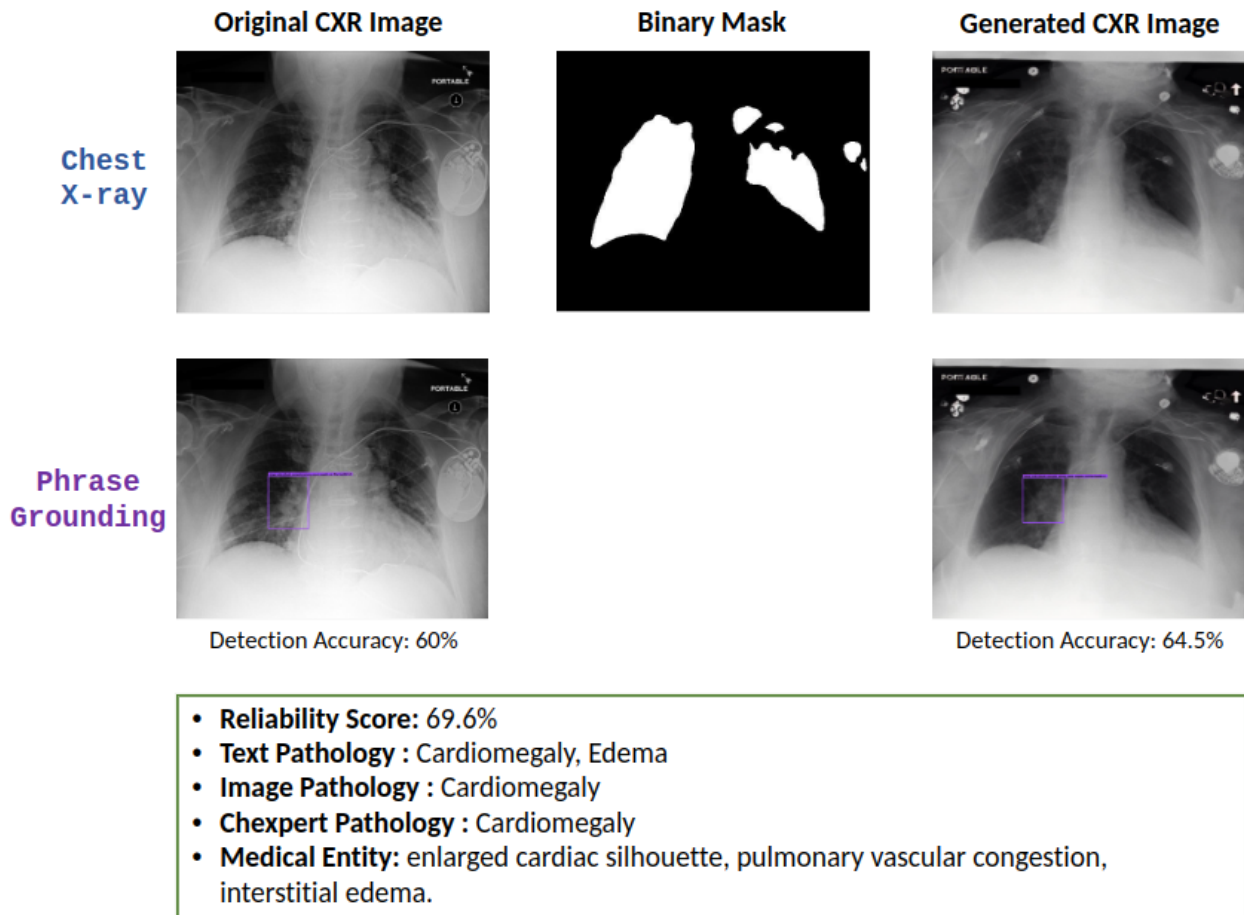


Figure 10: An example output of our pipeline.

Regarding feature similarity using χ^2 , analysis across 1901 samples showed the following observations:

- 407 samples had low localization probabilities for both the original and random reports, rendering the results inconclusive.
- 396 samples showed valid localization only when using the original report.
- 431 samples produced more acceptable localization results with the random report compared to the original report.
- 667 samples demonstrated significantly lower χ^2 values for the original report compared to the random report, indicating better feature correspondence.

Although there were 431 cases where the localization model failed to detect regions accurately based on the original report, the pipeline's performance is evident. Even in these cases, the average χ^2 value for regions localized using the random report was relatively high, reflecting the system's ability to identify and highlight dissimilarities between false report segments in generated and original images. This underscores the robustness and sensitivity of the pipeline, even when faced with similarities in the pathology.

Finally, we present the results for each pathology class. Figure 12 illustrates the frequency of each pathology in our test dataset. The most frequent occurrences are observed for "Lung Opacity" and "Pleural Effusion," followed by "Cardiomegaly" and "Edema."

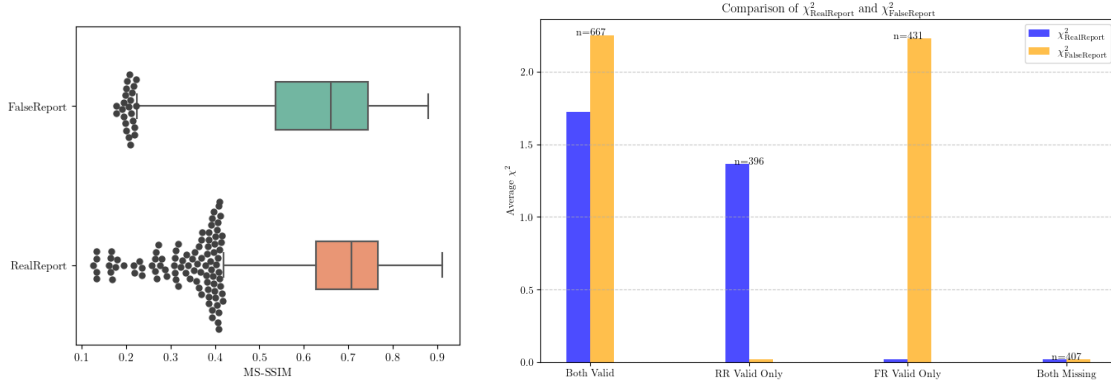


Figure 11: The similarity comparison between the localization and the generated CXR images was evaluated using MS-SSIM and χ^2 calculations based on two text inputs: the Real Report (RR), which represents the ground truth associated with the CXR image, and a False Report (FR), which has no correlation with the RR. The χ^2 plot on the left categorizes the results into four scenarios based on the output of the phrase grounding model: Both RR and FR produce valid localizations, only RR produces a valid localization, only FR produces a valid localization, neither RR nor FR yields a valid localization. The MS-SSIM boxplot on the right illustrates the distribution of similarity scores for each scenario, showing the density of evaluation for both the real and false reports.

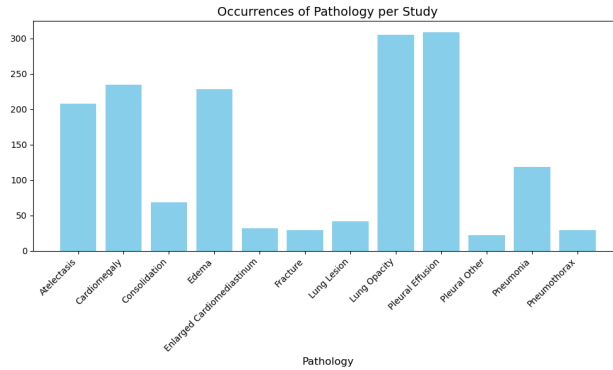


Figure 12: Occurrence of pathologies in the test dataset, includes 2018 studies. The most frequent occurrences are observed for “Lung Opacity” and “Pleural Effusion,” followed by “Cardiomegaly” and “Edema.”

For each pathology, we present the MS-SSIM score for each subject in Figure 13. The results show that the highest average scores are associated with “Lung Lesion” and “Fracture”. Although these pathologies are less frequent in our test set, they are easier to interpret in a CXR image. Based on our findings, the most challenging pathologies to interpret in a CXR image are “Pneumonia”, “Pneumothorax”, and “Pleural others”. Among these, “Pneumonia” occurs more frequently but remains the most difficult to assess. Additionally, our results indicate that “Edema” is the most ambiguous class, as it shows the highest variability. This variability could be attributed to the subtle and often similarity in the nature of the symptoms in CXR images, which may lead to difficulty in distinguishing it from each other. Our overall findings suggest that this interpretive study is crucial for enhancing the understanding and reliability of AI-generated reports. A few case studies are presented in Appendix A to further demonstrate the effectiveness of our VICCA model.

6 Conclusion

Recent advancements in chest X-ray radiology have prioritized enhancing interpretability, with a significant reliance on large language models for automated report generation. While these models show promising performance, occasional inaccuracies in their predictions limit their clinical applicability. This research introduces a novel approach to achieving a high degree of interpretability by leveraging AI-driven metrics and perspectives that mimic radiologist evaluations without the need for human feedback.

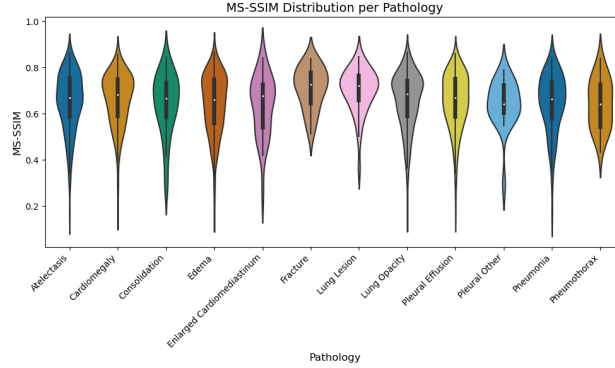


Figure 13: The MS-SSIM distribution per pathology in the test dataset.

Our framework demonstrates that combining multiple AI models can enhance interpretability by offering visual explanations with confidence scores for localization and introducing interpretative metrics for ROI through generative models. This approach not only supports radiologists by offering AI-assisted for generated reports but also aids general practitioners in areas with limited access to expert radiologists, improving decision-making and patient care and ultimately improving patient outcomes on a broader scale. Additionally, our model serves as a valuable tool for researchers aiming to improve their report generation models.

In this project, we introduce not just a multimodal pipeline of different AI models, but our work represents a significant step forward in the application of AI to chest X-ray radiology by introducing a concept of collaborative AI decision-making and enhancing the interpretability of their outputs. Our proposed training strategy integrates multiple tasks and datasets, presenting a viable approach to achieve this goal. By leveraging diverse AI models and their respective strengths, we create a robust framework that can provide comprehensive insights and support across various clinical scenarios.

7 Code Repository

Results can be reproduced using the code available in the GitHub repository <https://github.com/sayeh1994/vicca.git>. The code will be accessible after submission.

8 Acknowledgment

We want to acknowledge that all the computations presented in this paper were performed using the Gricad infrastructure (<https://gricad.univ-grenoble-alpes.fr>), which is supported by Grenoble research communities.

References

- Nur Yildirim, Hannah Richardson, Maria Teodora Wetscherek, Junaid Bajwa, Joseph Jacob, Mark A. Pinnock, Stephen Harris, Daniel Coelho De Castro, Shruthi Bannur, Stephanie L. Hyland, Pratik Ghosh, Mercy Prasanna Ranjit, Kenza Bouzid, Anton Schwaighofer, Fernando P'erez-Garc'ia, Harshita Sharma, Ozan Oktay, Matthew P. Lungren, Javier Alvarez-Valle, Aditya Nori, and Anja Thieme. Multimodal healthcare ai: Identifying and designing clinically relevant vision-language applications for radiology. *Proceedings of the CHI Conference on Human Factors in Computing Systems*, 2024. URL <https://api.semanticscholar.org/CorpusID:267783109>.
- Xieling Chen, Haoran Xie, Xiaohui Tao, Fu Lee Wang, Mingming Leng, and Baiying Lei. Artificial intelligence and multimodal data fusion for smart healthcare: topic modeling and bibliometrics. *Artificial Intelligence Review*, 57(4): 91, 2024.
- Philip Müller, Georgios Kaissis, and Daniel Rueckert. Chex: Interactive localization and region description in chest x-rays, 2024.
- Shruthi Bannur, Kenza Bouzid, Daniel Coelho de Castro, Anton Schwaighofer, Sam Bond-Taylor, Maximilian Ilse, Fernando Pérez-García, Valentina Salvatelli, Harshita Sharma, Felix Meissen, Mercy Ranjit, Shaury Srivastav, Julia Gong, Fabian Flack, Ozan Oktay, Anja Thieme, Matthew P Lungren, Maria Teodora Wetscherek, Javier

- Alvarez-Valle, and Stephanie Hyland. Maira-2: Grounded radiology report generation. Technical Report MSR-TR-2024-18, Microsoft, June 2024. URL <https://www.microsoft.com/en-us/research/publication/maira-2-grounded-radiology-report-generation/>.
- Beddiar Romaiassa, Mourad Oussalah, Tapio Seppänen, and Rachid Jennane. Acapmed: Automatic captioning for medical imaging. *Applied Sciences*, 12, 11 2022. doi: 10.3390/app122111092.
- Alexander Selivanov, Oleg Y. Rogov, Daniil Chesakov, Artem Shelmanov, Irina Fedulova, and Dmitry V. Dylov. Medical image captioning via generative pretrained transformers. *Scientific Reports*, 13(1):4171, Mar 2023. ISSN 2045-2322. doi: 10.1038/s41598-023-31223-5. URL <https://doi.org/10.1038/s41598-023-31223-5>.
- Benedikt Boecking, Naoto Usuyama, Shruthi Bannur, Daniel Coelho de Castro, Anton Schwaighofer, Stephanie Hyland, Maria Teodora Wetscherek, Tristan Naumann, Aditya Nori, Javier Alvarez-Valle, Hoifung Poon, and Ozan Oktay. Making the most of text semantics to improve biomedical vision-language processing. In *The European Conference on Computer Vision (ECCV)*, October 2022.
- Shih-Cheng Huang, Liyue Shen, Matthew P. Lungren, and Serena Yeung. Gloria: A multimodal global-local representation learning framework for label-efficient medical image recognition. In *2021 IEEE/CVF International Conference on Computer Vision (ICCV)*, pages 3922–3931, 2021. doi: 10.1109/ICCV48922.2021.00391.
- Tim Tanida, Philip Müller, Georgios Kaissis, and Daniel Rueckert. Interactive and explainable region-guided radiology report generation. In *CVPR*, 2023.
- Joseph Paul Cohen, Joseph D. Viviano, Paul Bertin, Paul Morrison, Parsa Torabian, Matteo Guarrera, Matthew P Lungren, Akshay Chaudhari, Rupert Brooks, Mohammad Hashir, and Hadrien Bertrand. TorchXRrayVision: A library of chest X-ray datasets and models. In *Medical Imaging with Deep Learning*, 2022. URL <https://github.com/mlmed/torchxrayvision>.
- Sayeh Gholipour Picha, Dawood Al Chanti, and Alice Caplier. Semantic textual similarity assessment in chest x-ray reports using a domain-specific cosine-based metric. In *Proceedings of the 17th International Joint Conference on Biomedical Engineering Systems and Technologies - Volume 1: BIOINFORMATICS*, pages 487–494. INSTICC, SciTePress, 2024. ISBN 978-989-758-688-0. doi: 10.5220/0012429600003657.
- Jacob Devlin, Ming-Wei Chang, Kenton Lee, and Kristina Toutanova. Bert: Pre-training of deep bidirectional transformers for language understanding. In *North American Chapter of the Association for Computational Linguistics*, 2019. URL <https://api.semanticscholar.org/CorpusID:52967399>.
- Prafulla Dhariwal and Alexander Nichol. Diffusion models beat gans on image synthesis. In M. Ranzato, A. Beygelzimer, Y. Dauphin, P.S. Liang, and J. Wortman Vaughan, editors, *Advances in Neural Information Processing Systems*, volume 34, pages 8780–8794. Curran Associates, Inc., 2021. URL https://proceedings.neurips.cc/paper_files/paper/2021/file/49ad23d1ec9fa4bd8d77d02681df5cfa-Paper.pdf.
- Lvmin Zhang, Anyi Rao, and Maneesh Agrawala. Adding conditional control to text-to-image diffusion models, 2023.
- Zhihao Chen, Yang Zhou, Anh Tran, Junting Zhao, Liang Wan, Gideon Su Kai Ooi, Lionel Tim-Ee Cheng, Choon Hua Thng, Xinxing Xu, Yong Liu, and Huazhu Fu. Medical phrase grounding with region-phrase context contrastive alignment. In Hayit Greenspan, Anant Madabhushi, Parvin Mousavi, Septimiu Salcudean, James Duncan, Tanveer Syeda-Mahmood, and Russell Taylor, editors, *Medical Image Computing and Computer Assisted Intervention – MICCAI 2023*, pages 371–381, Cham, 2023. Springer Nature Switzerland. ISBN 978-3-031-43990-2.
- Konstantinos Vilouras, Pedro Sanchez, Alison Q. O’Neil, and Sotirios A. Tsaftaris. Zero-shot medical phrase grounding with off-the-shelf diffusion models, 2024. URL <https://arxiv.org/abs/2404.12920>.
- Akimichi Ichinose, Taro Hatsutani, Keigo Nakamura, Yoshiro Kitamura, Satoshi Iizuka, Edgar Simo-Serra, Shoji Kido, and Noriyuki Tomiyama. Visual grounding of whole radiology reports for 3d ct images. In Hayit Greenspan, Anant Madabhushi, Parvin Mousavi, Septimiu Salcudean, James Duncan, Tanveer Syeda-Mahmood, and Russell Taylor, editors, *Medical Image Computing and Computer Assisted Intervention – MICCAI 2023*, pages 611–621, Cham, 2023. Springer Nature Switzerland. ISBN 978-3-031-43904-9.
- Ke Zou, Yang Bai, Zhihao Chen, Yang Zhou, Yidi Chen, Kai Ren, Meng Wang, Xuedong Yuan, Xiaojing Shen, and Huazhu Fu. Medrg: Medical report grounding with multi-modal large language model, 2024.
- Shilong Liu, Zhaoyang Zeng, Tianhe Ren, Feng Li, Hao Zhang, Jie Yang, Chunyuan Li, Jianwei Yang, Hang Su, Jun Zhu, et al. Grounding dino: Marrying dino with grounded pre-training for open-set object detection. *arXiv preprint arXiv:2303.05499*, 2023.
- Pierre Chambon, Christian Bluethgen, Jean-Benoit Delbrouck, Rogier Van der Sluijs, Małgorzata Połacin, Juan Manuel Zambrano Chaves, Tanishq Mathew Abraham, Shivanshu Purohit, Curtis P. Langlotz, and Akshay Chaudhari. Roentgen: Vision-language foundation model for chest x-ray generation, 2022a. URL <https://arxiv.org/abs/2211.12737>.

- Tobias Weber, Michael Ingrisch, Bernd Bischl, and David Rügamer. Cascaded latent diffusion models for high-resolution chest x-ray synthesis. In *Advances in Knowledge Discovery and Data Mining: 27th Pacific-Asia Conference, PAKDD 2023*. Springer, 2023.
- Pierre Joseph Marcel Chambon, Christian Bluethgen, Curtis Langlotz, and Akshay Chaudhari. Adapting pretrained vision-language foundational models to medical imaging domains. In *NeurIPS 2022 Foundation Models for Decision Making Workshop*, 2022b. URL <https://openreview.net/forum?id=QtxbYdJVT8Q>.
- Robin Rombach, A. Blattmann, Dominik Lorenz, Patrick Esser, and Björn Ommer. High-resolution image synthesis with latent diffusion models. *2022 IEEE/CVF Conference on Computer Vision and Pattern Recognition (CVPR)*, pages 10674–10685, 2021. URL <https://api.semanticscholar.org/CorpusID:245335280>.
- Kai Packhäuser, Lukas Folle, Florian Thamm, and Andreas Maier. Generation of anonymous chest radiographs using latent diffusion models for training thoracic abnormality classification systems, 2022.
- Sayeh Gholipour Picha., Dawood Al Chanti., and Alice Caplier. How far generated data can impact neural networks performance? In *Proceedings of the 18th International Joint Conference on Computer Vision, Imaging and Computer Graphics Theory and Applications - Volume 5: VISAPP*, pages 472–479. INSTICC, SciTePress, 2023. ISBN 978-989-758-634-7. doi: 10.5220/0011629000003417.
- Anees Ur Rehman Hashmi, Ibrahim Almakky, Mohammad Areeb Qazi, Santosh Sanjeev, Vijay Ram Papineni, Dwarikanath Mahapatra, and Mohammad Yaqub. Xreal: Realistic anatomy and pathology-aware x-ray generation via controllable diffusion model. *arXiv preprint arXiv:2403.09240*, 2024.
- Ha Q. Nguyen, Khanh Lam, Linh T. Le, Hieu H. Pham, Dat Q. Tran, Dung B. Nguyen, Dung D. Le, Chi M. Pham, Hang T. T. Tong, Diep H. Dinh, Cuong D. Do, Luu T. Doan, Cuong N. Nguyen, Binh T. Nguyen, Que V. Nguyen, Au D. Hoang, Hien N. Phan, Anh T. Nguyen, Phuong H. Ho, Dat T. Ngo, Nghia T. Nguyen, Nhan T. Nguyen, Minh Dao, and Van Vu. Vindr-cxr: An open dataset of chest x-rays with radiologist’s annotations, 2022. URL <https://arxiv.org/abs/2012.15029>.
- Nicolas Carion, Francisco Massa, Gabriel Synnaeve, Nicolas Usunier, Alexander Kirillov, and Sergey Zagoruyko. End-to-end object detection with transformers. In Andrea Vedaldi, Horst Bischof, Thomas Brox, and Jan-Michael Frahm, editors, *Computer Vision – ECCV 2020*, pages 213–229, Cham, 2020. Springer International Publishing. ISBN 978-3-030-58452-8.
- Joy T. Wu, Nkechinyere N. Agu, Ismini Lourentzou, Arjun Sharma, Joseph Alexander Paguio, Jasper Seth Yao, Edward Christopher Dee, William Mitchell, Satyananda Kashyap, Andrea Giovannini, Leo Anthony Celi, and Mehdi Moradi. Chest imagenome dataset for clinical reasoning. *ArXiv*, abs/2108.00316, 2021. URL <https://api.semanticscholar.org/CorpusID:235420881>.
- Kexin Huang, Jaan Altosaar, and Rajesh Ranganath. Clinicalbert: Modeling clinical notes and predicting hospital readmission. *arXiv:1904.05342*, 2019.
- Kaiming He, Xiangyu Zhang, Shaoqing Ren, and Jian Sun. Deep residual learning for image recognition. In *2016 IEEE Conference on Computer Vision and Pattern Recognition (CVPR)*, pages 770–778, 2016. doi: 10.1109/CVPR.2016.90.
- Ze Liu, Yutong Lin, Yue Cao, Han Hu, Yixuan Wei, Zheng Zhang, Stephen Lin, and Baining Guo. Swin transformer: Hierarchical vision transformer using shifted windows. In *Proceedings of the IEEE/CVF International Conference on Computer Vision (ICCV)*, 2021.
- Haotian Zhang, Pengchuan Zhang, Xiaowei Hu, Yen-Chun Chen, Liunian Harold Li, Xiyang Dai, Lijuan Wang, Lu Yuan, Jenq-Neng Hwang, and Jianfeng Gao. GLIPv2: Unifying localization and vision-language understanding. In Alice H. Oh, Alekh Agarwal, Danielle Belgrave, and Kyunghyun Cho, editors, *Advances in Neural Information Processing Systems*, 2022. URL <https://openreview.net/forum?id=wiBEFdv18L>.
- Tsung-Yi Lin, Priya Goyal, Ross B. Girshick, Kaiming He, and Piotr Dollár. Focal loss for dense object detection. *2017 IEEE International Conference on Computer Vision (ICCV)*, pages 2999–3007, 2017. URL <https://api.semanticscholar.org/CorpusID:47252984>.
- Alistair E. W. Johnson, Tom J. Pollard, Nathaniel R. Greenbaum, Matthew P. Lungren, Chih ying Deng, Yifan Peng, Zhiyong Lu, Roger G. Mark, Seth J. Berkowitz, and Steven Horng. Mimic-cxr-jpg, a large publicly available database of labeled chest radiographs, 2019a.
- Jiajun Deng, Zhengyuan Yang, Tianlang Chen, Wengang Zhou, and Houqiang Li. Transvg: End-to-end visual grounding with transformers. *arXiv preprint arXiv:2104.08541*, 2021.
- A L Goldberger, L A Amaral, L Glass, J M Hausdorff, P C Ivanov, R G Mark, J E Mietus, G B Moody, C K Peng, and H E Stanley. PhysioBank, PhysioToolkit, and PhysioNet: components of a new research resource for complex physiologic signals. *Circulation*, 101(23):E215–20, June 2000.

Jeremy Irvin, Pranav Rajpurkar, Michael Ko, Yifan Yu, Silvana Ciurea-Ilcus, Chris Chute, Henrik Marklund, Behzad Haghgoo, Robyn Ball, Katie Shpanskaya, Jayne Seekins, David A. Mong, Safwan S. Halabi, Jesse K. Sandberg, Ricky Jones, David B. Larson, Curtis P. Langlotz, Bhavik N. Patel, Matthew P. Lungren, and Andrew Y. Ng. Chexpert: A large chest radiograph dataset with uncertainty labels and expert comparison, 2019. URL <https://doi.org/10.71718/y7pj-4v93>.

Gricad. infrastructure supported by grenoble research communities. URL <https://gricad.univ-grenoble-alpes.fr>.

Alistair E. W. Johnson, Tom J. Pollard, Seth J. Berkowitz, Nathaniel R. Greenbaum, Matthew P. Lungren, Chih-ying Deng, Roger G. Mark, and Steven Horng. Mimic-cxr, a de-identified publicly available database of chest radiographs with free-text reports. *Scientific Data*, 6(1):317, Dec 2019b. ISSN 2052-4463. doi: 10.1038/s41597-019-0322-0. URL <https://doi.org/10.1038/s41597-019-0322-0>.

Original Prompt

Left lower lobe atelectasis predominantly posterior basal segment and small left pleural effusion. Left lower lobe has partially expanded, reflected in return of the mediastinum to the midline, but there is still atelectasis and small residual left pleural effusion, a common accompaniment to lower lobe atelectasis, particularly in elderly patients.

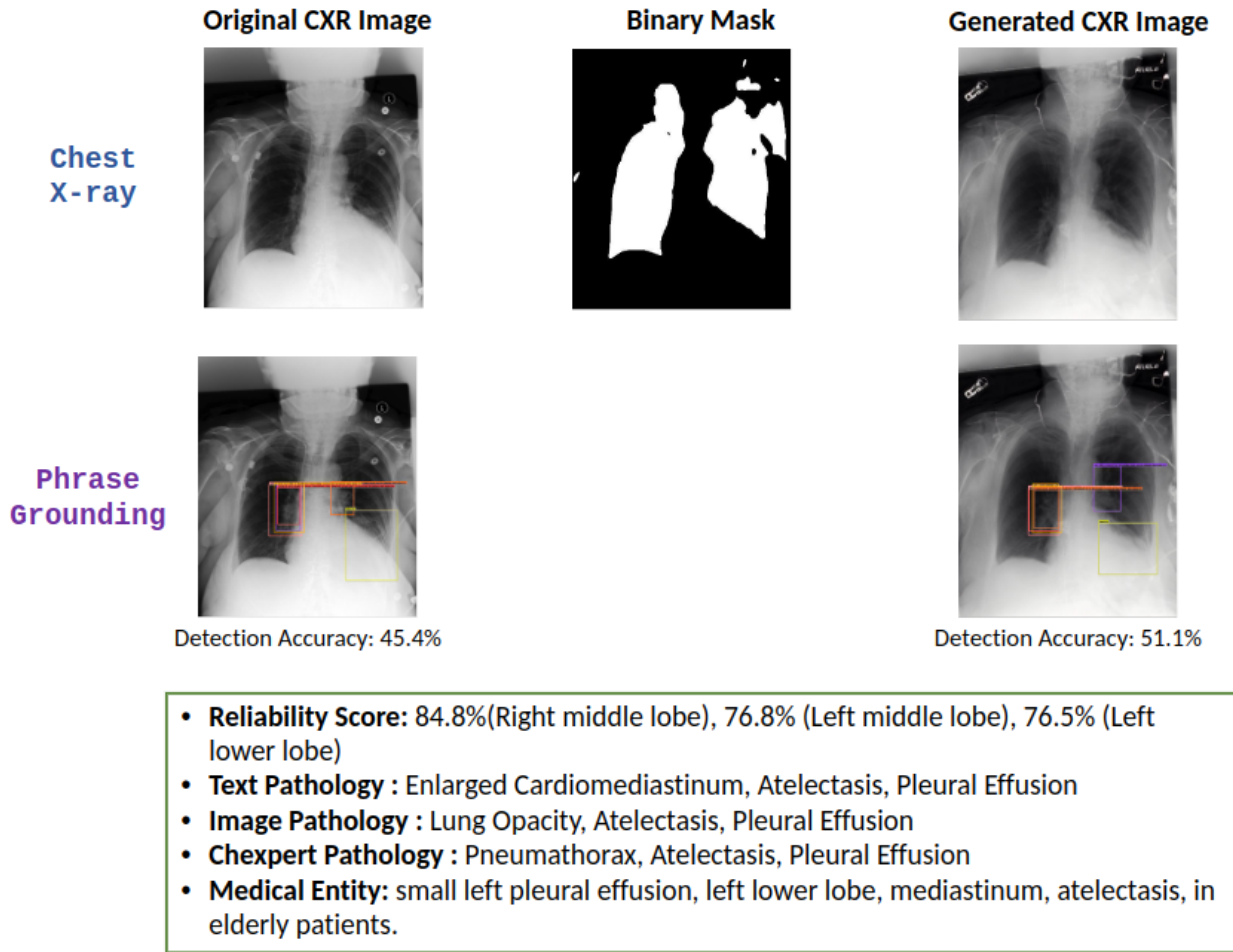


Figure 14: Case 1: Multiple Pathology

A Case Study

We present various scenarios and examples encountered during our study to illustrate the application and performance of our project. These include both successful cases and failed cases, which are included to provide deeper insights and facilitate a better understanding of the limitations and challenges of the approach.

A.1 Case 1: Multiple Pathology

In the first scenario presented in figure 14, we examine a case involving multiple pathologies in both the text prompt and the image. Using our phrase grounding visualization, we identified three regions of interest (ROIs) in both the original and generated images. Although the detection probabilities were relatively low, the high similarity between the corresponding ROIs across both images indicates that the prompt can be considered trustworthy. Additionally, the pathologies identified through the prompt and the image using an AI model closely align with the Chexpert annotations derived from the MIMIC-CXR dataset Johnson et al. [2019b].

A.2 Case 2: Single Pathology A Success Case

In the second case, presented in Figure 15, we analyze a scenario involving a single pathology. While two pathologies were initially identified in the text prompt, both our image-based pathology detection and the Chexpert annotation

Original Prompt

Enlarged cardiac silhouette is accompanied by pulmonary vascular congestion and diffuse interstitial edema.

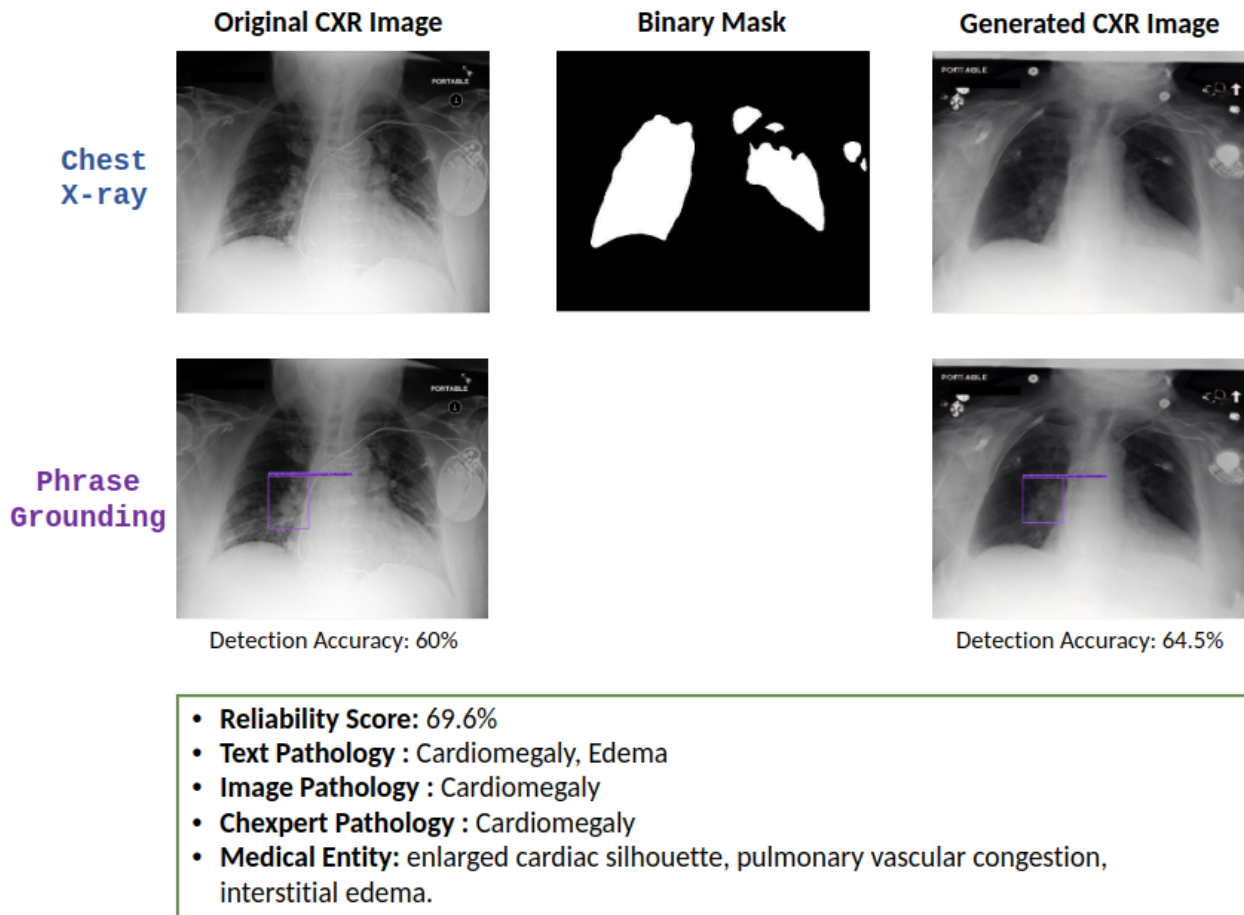


Figure 15: Case 2: Single Pathology A Success Case

confirm the presence of only one pathology, maintaining consistency across methods. Moreover, our phrase grounding accurately detected a single pathology, which exhibits a high similarity with the pathology described in the prompt through the generated image. This alignment demonstrates that the prompt is consistent with the image and can be considered trustworthy.

A.3 Case 3: Single Pathology A Failure Case

In contrast to the previous case, Figure 16 illustrates a failure to correctly align the original prompt with the corresponding image. Phrase grounding on the original CXR image detected only one region of interest (ROI) associated with a pathology, whereas pathology detection identified three distinct pathologies in the image. Similarly, the generated image from the same prompt revealed two ROIs, but their similarity scores with the original image were notably low.

While the AI model identified only one pathology from the text, this pathology corresponded to one of the detected pathologies in the image. However, these results did not align with the annotated pathologies in the dataset. Despite the prompt being originally written by a radiologist, the system failed to reliably associate it with the correct CXR image. This case highlights challenges in ensuring consistency and accuracy across modalities when relying solely on automated approaches without any interpretation.

Original Prompt

Pulmonary vascular congestion and platelike atelectasis in the left midlung, reflecting exceedingly low lung volumes. Low lung volumes exaggerate vascular crowding and possible interstitial edema in the left lung.

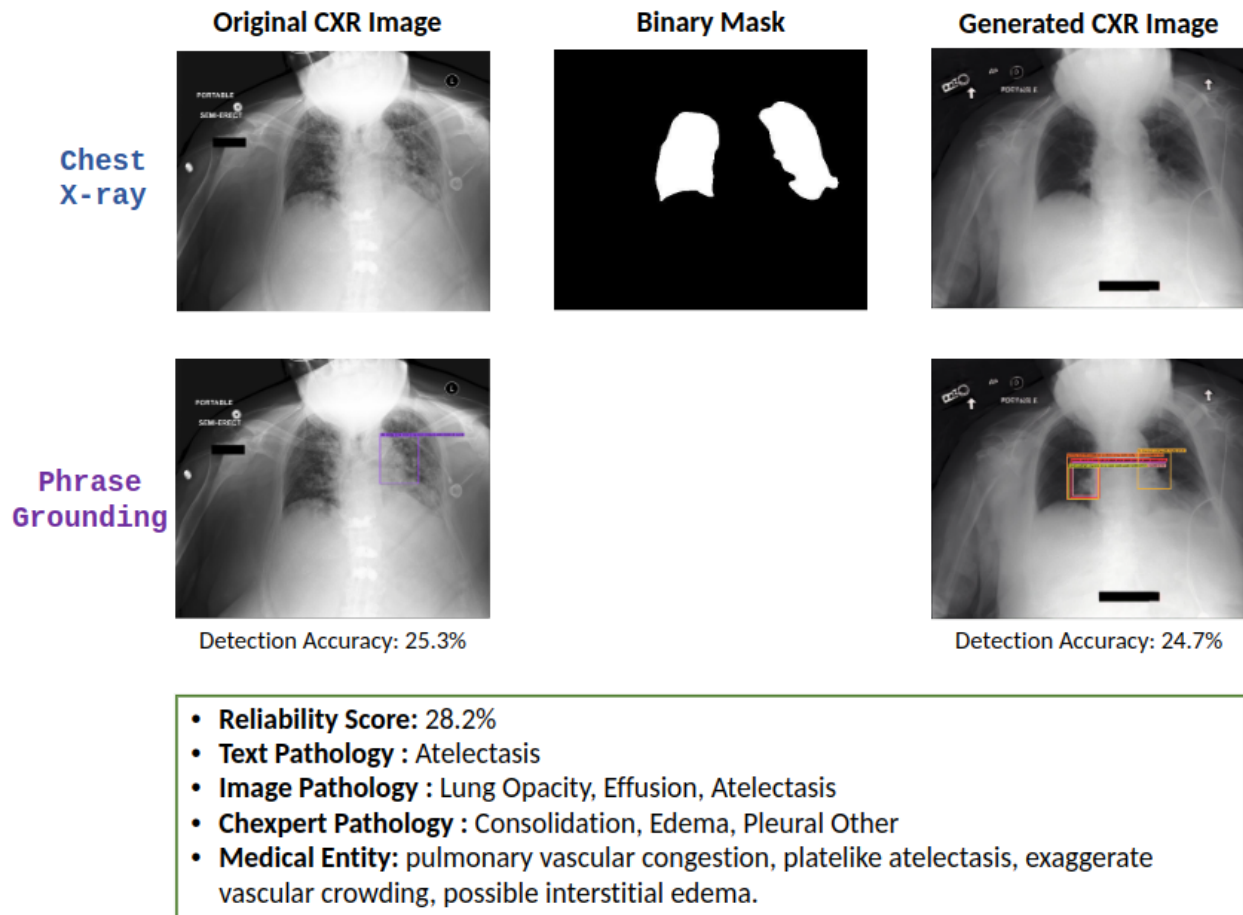


Figure 16: Case 3: Single Pathology A Failure Case

A.4 Case 4: A Success Case of Using False Report

In this case which is illustrated in Figure 17, we examine a scenario where the prompt differs significantly from the original dataset prompt and shows no correlation with it. Although phrase grounding on the original CXR image identified a region of interest (ROI) corresponding to the prompt, but no ROIs were detected when applying phrase grounding on the generated image.

Pathology detection from the text was entirely misaligned with the pathologies identified in the image, and the similarity score between the detected ROI in the original image and the corresponding region in the generated image is notably low. Furthermore, the annotated pathology from Chexpert differed substantially. For instance, while the annotation did not include “pleural effusion” and instead noted only “edema,” the original report clearly indicated the presence of “pleural effusion.”

This case highlights two key insights: (1) even trusted annotations can occasionally lack accuracy or completeness, and (2) the model demonstrated robustness by not incorrectly aligning this mismatched prompt with the given CXR image. This underscores the importance of incorporating our approach to ensure reliability and trustworthiness in automated systems.

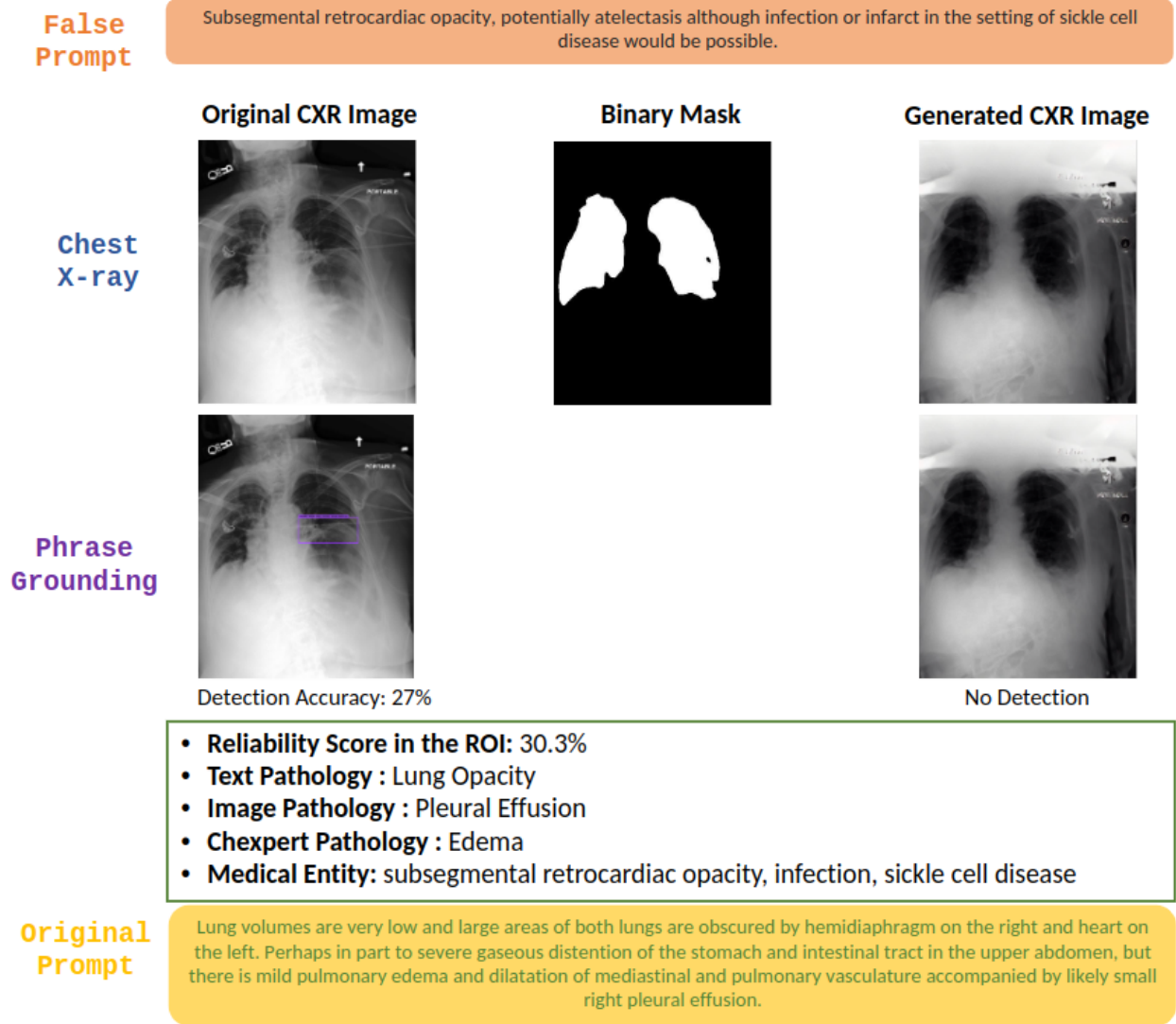


Figure 17: Case 4: A Success Case of Using False Report

A.5 Case 5: No Pathology

In our final case, we examine an instance where the original annotation indicates no pathology. While the report describes a ROI in the image, our phrase grounding model detects an anomaly within the ROI in both the generated and original images. The reliability score indicates a high degree of similarity, but the detection accuracy score is notably low. Additionally, our image classification model identifies a pathology for this image.

Upon closer inspection of the text prompt, we observe a probable diagnosis linked to the ROI. Although the official annotation suggests no pathology, the findings from our model highlight potential ambiguity. This case could be considered inconclusive, as the report itself is somewhat ambiguous, complicating the decision-making process.

Original Prompt

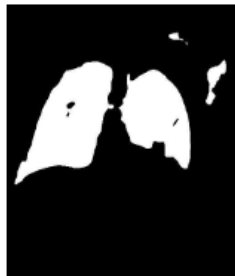
Allowing for the portable technique, the cardiac silhouette may be mildly enlarged. Obliquity of the patient is probably responsible for the apparent displacement of the heart into the left hemithorax.

Chest X-ray

Original CXR Image



Binary Mask



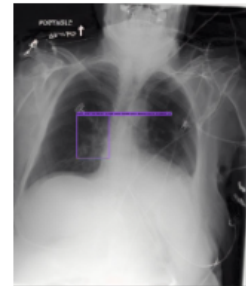
Generated CXR Image



Phrase Grounding



Detection Accuracy: 24%



Detection Accuracy: 26%

- **Reliability Score:** 71%
- **Text Pathology :** No Finding
- **Image Pathology :** Effusion
- **Chexpert Pathology :** No Finding
- **Medical Entity:** cardiac silhouette, mildly enlarged, displacement of the heart , the left hemithorax.

Figure 18: Case 5: No Pathology